Mesoscale Modelling of a Masonry Building Subjected to Earthquake Loading

Corrado CHISARI[1], Lorenzo MACORINI[2], Bassam A. IZZUDDIN[3]

Abstract

Masonry structures constitute an important part of the built environment and architectural heritage in seismic areas. A large number of these old structures showed inadequate performance and suffered substantial damage under past earthquakes. Realistic numerical models are required for accurate response predictions and for addressing the implementation of effective strengthening solutions. A comprehensive mesoscale modelling strategy explicitly allowing for masonry bond is presented in this paper. It is based upon advanced nonlinear material models for interface elements simulating cracks in mortar joints and brick/block units under cyclic loading. Moreover, domain decomposition and mesh tying techniques are used to enhance computational efficiency in detailed nonlinear simulations. The potential of this approach is shown with reference to a case study of a full-scale unreinforced masonry building previously tested in laboratory under pseudo-dynamic loading. The results obtained confirm that the proposed modelling strategy for brick/block-masonry structures leads to accurate representations of the seismic response of 3D building structures, both at the local and global levels. The numerical-experimental comparisons show that this detailed modelling approach

[1]Marie Skłodowska-Curie Individual Fellow, Department of Civil and Environmental Engineering, Imperial College London, United Kingdom. Currently, Assistant professor, Department of Architecture and Industrial Design, University of Campania "Luigi Vanvitelli", corrado.chisari@unicampania.it

[2]Senior Lecturer, Department of Civil and Environmental Engineering, Imperial College London, United Kingdom, l.macorini@imperial.ac.uk

[3]Professor of Computational Structural Mechanics, Department of Civil and Environmental Engineering, Imperial College London, United Kingdom, b.izzuddin@imperial.ac.uk

enables remarkably accurate predictions of the actual dynamic characteristics, along with the main resisting mechanisms and crack patterns.

Keywords: Mesoscale masonry modelling; Zero-thickness interface; Nonlinear dynamic analysis; Mesh tying; Hierarchic partitioning.

1 Introduction

The seismic behaviour of unreinforced masonry (URM) structures including buildings and bridges is very complex and characterised by material nonlinearities even at low loading levels. This is due to the heterogeneity of masonry in which two components, namely mortar joints and units, are connected giving rise to a meso-structure of non-negligible size compared to the dimensions of typical masonry wall elements. Furthermore, the individual mechanical properties of mortar and units are characterised by low tensile strength and quasi-brittle behaviour as well as non-rigid and potentially weak adhesion between them. With the aim of obtaining accurate predictions of the mechanical response of masonry members and structures, several numerical strategies for nonlinear analysis have been developed over the last two decades mainly in the context of the finite element method (FEM). These include micro- or mesoscale models (Lourenço & Rots, 1997; Gambarotta & Lagomarsino, 1997; Macorini & Izzuddin, 2011) where the individual masonry constituents are modelled separately, and macroscale models (Lourenço, 1996; Berto, et al., 2002; Pantò, et al., 2016) which represent masonry as a homogeneous material. Interest has also been gained by mixed methods based on homogenisation, where the mechanical behaviour at the macroscale is obtained by the solution of a sub-problem at the microscale (Anthoine, 1995; Massart, et al., 2007; Luciano & Sacco, 1997; Addessi & Sacco, 2016).

In mesoscale masonry models the contributions of both mortar and brick-mortar interfaces are lumped together and explicitly represented using zero-thickness nonlinear interface elements. This enables the analyst to account also for damage-induced anisotropy achieving realistic predictions of crack propagation within any masonry element (Macorini & Izzuddin, 2011). Similar interface elements with different mechanical properties can also be used to simulate failure in bricks (Lourenço & Rots, 1997; Macorini & Izzuddin, 2011). The advantage of such an approach is that individual component properties can be calibrated by means of simple tests on small scale specimens or more advanced inverse analysis techniques considering the response of a representative part of the analysed structure subjected to specific loading conditions (Sarhosis & Sheng, 2014; Chisari, et al., 2015; Chisari, et al., 2018). Accurate predictions of cracking patterns and global responses can be achieved for both in-plane and out-of-plane loading. However, a high computational cost is typically associated with the fine discretisation needed to represent the masonry bond, thus the application of mesoscale modelling approach has been limited to single walls (Macorini & Izzuddin, 2011) or arches (Zhang, et al., 2016), and only recently to masonry bridges (Tubaldi, et al., 2018), framed structures with masonry infill (Macorini & Izzuddin, 2014) and small masonry buildings (D'Altri, et al., 2019).

In recent works, time-history seismic analysis of buildings has been generally performed by means of homogenised isotropic representations of masonry (Betti, et al., 2015; Mendes & Lourenço, 2014; Valente & Milani, 2019), even though the preferred approaches still rely on further simplifications regarding the numerical representation, e.g. macro-models (Lagomarsino, et al., 2013; Kim & White, 2004), or the analysis type, e.g. nonlinear static analysis (Milani & Valente, 2015; D'Ayala & Ansal, 2012; Endo, et al., 2017). Very few papers directly compare experimental results with the numerical outcomes for entire URM buildings subjected to seismic loading (Betti, et al., 2014; Mandirola, et al., 2016; Kallioras, et al., 2019), and none of them makes use of detailed mesoscale descriptions. It is important thus to investigate the effectiveness of this latter approach, even with regard to the possibility of calibrating material parameters with standard experimental tests and the computational feasibility of modelling large number of degrees of freedom.

In this paper, the mesoscale modelling strategy developed at Imperial College (Macorini & Izzuddin, 2011; Minga, et al., 2018) is used for the first time to investigate the dynamic response of a 3D masonry building structure under earthquake loading. The prediction of the structural response is based on the use of (i) an advanced material model for the cyclic behaviour of the interfaces representing cracks in bricks and in mortar, (ii) parallelisation of nonlinear structural analysis using hierarchic partitioning, and (iii) efficient mesh building and tying technique for non-conforming meshes. The results of a past research project including tests on single components, small assemblage and full-scale buildings under seismic actions are considered. In particular, shear tests on single walls, hammer tests for estimation of modal properties and pseudo-dynamic tests on the whole building prototype are all simulated, providing a strong basis for critical appraisal of the adopted modelling strategy.

2 Mesoscale modelling strategy for URM buildings

The mesoscale modelling approach used in this paper provides an accurate representation of the masonry components allowing for the specific masonry bond. Mortar and unit–mortar interfaces are modelled by 2D 16-noded zero-thickness nonlinear interface elements (Macorini & Izzuddin, 2011). Masonry units are represented by elastic 20-noded solid elements, and possible unit failure in tension and shear is accounted for by means of zero-thickness interface elements placed at the vertical mid-plane of each block (Figure 1). To do so, mortar joints are collapsed into the interfaces, while the solid elements are expanded. The discretisation for the structure, as proposed in (Macorini & Izzuddin, 2011), consists of two solid elements per brick connected by a brick-brick interface.

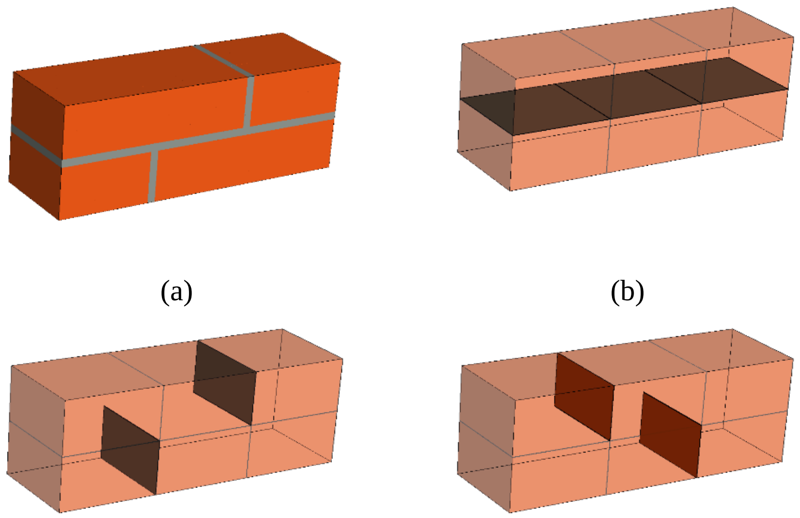

(a) (b) (c) (d)

Figure 1. Mesoscale modelling of masonry by means of solid elements for units (in transparency) and zero thickness interfaces: (a) real bond, (b) bed joints, (c) head joints, and (d) brick-brick interfaces.

Such requirements for meshing masonry elements lead to three main issues in the modelling of complex structures:

- The creation of the mesh for the building, with the accurate representation of the real masonry bond, may be involved and should ideally be performed in a semi-automatic way;
- The computational demand may easily become prohibitive for ordinary computational resources and hence requires advanced parallelisation of the calculations;
- Adjacent parts of the structure may entail different discretisation and thus the connection of them must be addressed. In particular, this is the case of orthogonal wall-wall and wall-floor connections.

In the following subsections, the adopted material model and the modelling strategy developed to consider these critical issues is described in more detail.

2.1 The material model for interfaces

The material model used for the 16-noded zero-thickness interfaces to simulate the response of both cracks in bricks and mortar joints is based on the coupling of plasticity and damage (Minga, et al., 2018). This approach is capable of simulating all the principal mechanical features of a mortar joint or a dry frictional interface, when mortar is absent, with an efficient formulation that ensures numerical robustness. In particular, it can simulate i) the softening behaviour in tension and shear, ii) the stiffness degradation depending on the level of damage, iii) the recovering of normal stiffness in compression following crack closure and iv) the permanent (plastic) strains at zero stresses when the interface is damaged.

In the elastic domain, the stress $\boldsymbol{\sigma}$ and displacement $\boldsymbol{u}$ vectors at the integration points are related by uncoupled stiffnesses:

$$\boldsymbol{\sigma} = \boldsymbol{k_0}\boldsymbol{u}$$
$$\boldsymbol{\sigma} = \{\tau_x, \tau_y, \sigma\}^T, \qquad \boldsymbol{u} = \{u_x, u_y, u_z\}^T, \boldsymbol{k_0} = \begin{bmatrix} k_V & 0 & 0 \\ 0 & k_V & 0 \\ 0 & 0 & k_N \end{bmatrix} \tag{1}$$

The yield criterion is represented in the stress space by a conical surface which simulates the behaviour in shear according to the Coulomb law, corresponding to mode II fracture. This surface, governed by cohesion c and friction angle φ, is capped by two planar surfaces representing failure in tension and compression respectively (Figure 2).

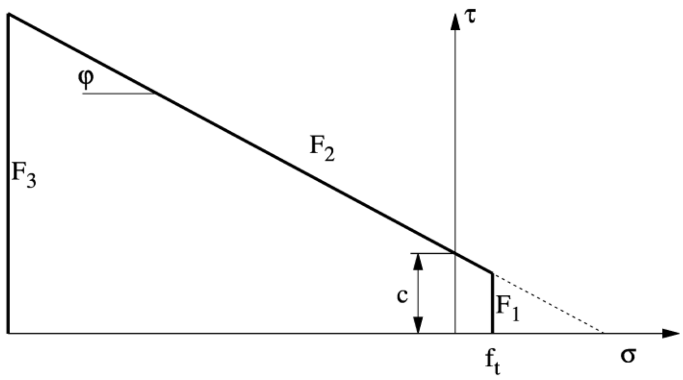

Figure 2. Multi-surface yield criterion (Minga, et al., 2018).

The evolution of the effective stresses is elastic perfectly-plastic, except for the case where the plastic surface F_1, representing failure in tension, is traversed. In this case, a hardening behaviour in the effective stress space is utilised. The softening behaviour in tension and compression in the nominal stress space is achieved by the introduction of damage. The damage of the interfaces is defined by a diagonal damage tensor $\boldsymbol{D}$ which controls stiffness degradation and is governed by the plastic work corresponding to each fracture mode, with three fracture energies assumed as material properties. By applying damage to the effective stresses $\tilde{\boldsymbol{\sigma}}$, corresponding to the physical stresses developed in the undamaged part of the interface, it is possible to obtain the nominal stresses $\boldsymbol{\sigma}$, defined as:

$$\boldsymbol{\sigma} = (\boldsymbol{I} - \boldsymbol{D})\tilde{\boldsymbol{\sigma}} = (\boldsymbol{I} - \boldsymbol{D})\boldsymbol{K}(\boldsymbol{\varepsilon} - \boldsymbol{\varepsilon}^{\boldsymbol{p}}) \quad (2)$$

In this way the implicit solution of the plastic problem and the damage evolution are decoupled, thus allowing for increased efficiency and robustness at the material level. A parameter μ governs the amount of plastic strain upon full unloading in tension, being 0.0 for a full damage model (no plastic strain at unloading) and 1.0 for maximum plastic strain consequent to the assumption of elastic-perfectly plastic effective stress-strain relationship. Further details about the material model may be found in (Minga, et al., 2018).

2.2 Hierarchic partitioning

The mesoscale approach described above is generally associated with significant computational cost, which may become excessive even for simulations of individual components or small structures (single walls) when using ordinary computational resources. To enable the analysis of large structures (multi-storey/multi-leaf walls or buildings), ADAPTIC (Izzuddin, 1991) utilises a domain decomposition method for nonlinear finite element analysis based on the concept of dual partition super-elements (Jokhio & Izzuddin, 2013; Jokhio & Izzuddin, 2015). In this method, domain decomposition is realised by replacing one or more subdomains in a "parent system" with a placeholder super-element, where the subdomains are processed separately as "child partitions", each wrapped by a dual super-element along the partition boundary. The analysis of the overall system, including the satisfaction of equilibrium and compatibility at all partition boundaries, is achieved through direct communication between all pairs of placeholder and dual super-elements.

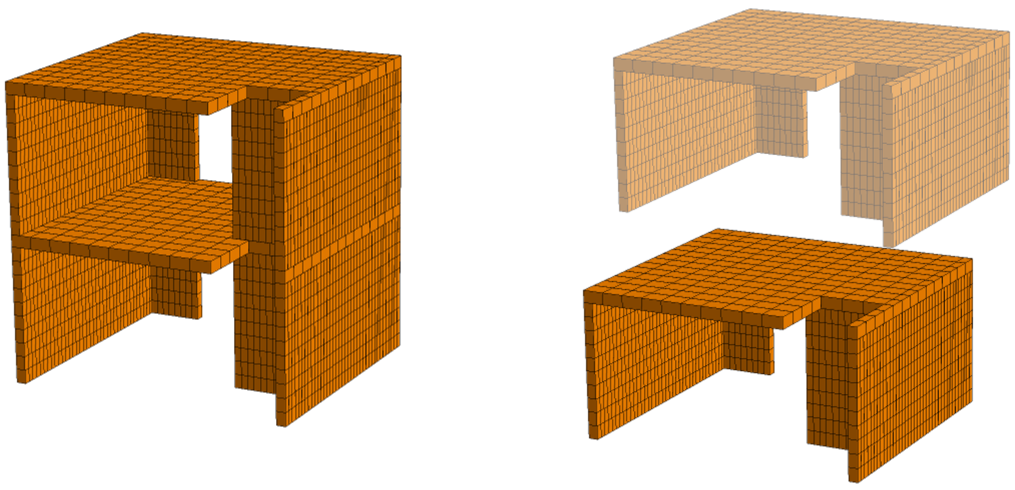

(a) (b)

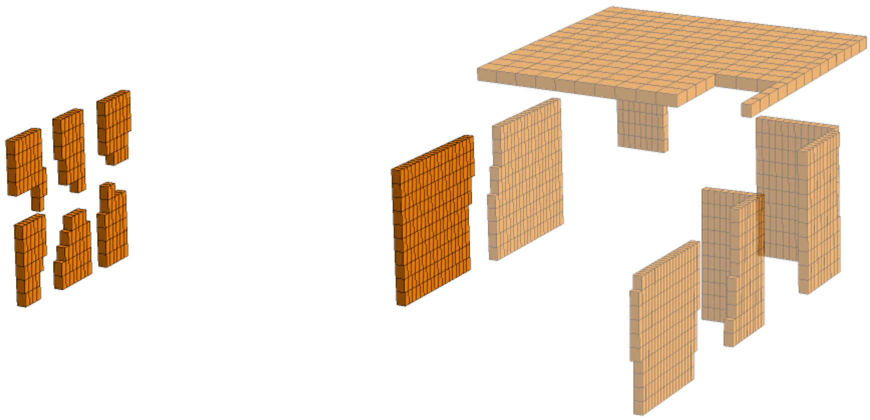

(d) (c)

Figure 3. Hierarchic partitioning of the building described in Section 3.2, in clockwise direction from the top left: (a) Level 0, (b) level 1, (c) level 2, and (d) level 3.

This approach allows for efficient parallelisation of the computational burden. However, it is easy to recognise that while for a small number of partitions the number of degrees of freedom (DOFs) of the children is larger than that of the parent, a greater number of child partitions increases the number of DOFs in the parent partition, which can ultimately represent the bottleneck of the analysis computing time.

This potential drawback of the original flat partitioning approach was discussed in (Macorini & Izzuddin, 2013) with reference to mesoscale partitioned simulations of large masonry components. It was confirmed that an excessive number of partitions implies greater computing demand at the parent structure level and high overheads relating to data communication, and that the most efficient subdivision with partitions can be achieved using partitions of the same or similar size (e.g. same number of nodes) and close to the size of the parent structure.

A further enhancement of the adopted domain decomposition strategy was developed in (Jokhio, 2012) introducing hierarchic partitioning, where several levels of partitioning are allowed. It was shown in (Macorini & Izzuddin, 2013) that for a masonry mesoscale model made of hundreds of thousand DOFs, such enhanced partitioning strategy leads to a speed-up up to ten times greater than flat partitioning while using the same number of processors. This approach is employed herein choosing “basic” child partitions for the structure, created from the global model by applying Metis partitioner (Karypis, 2015) implemented in the pre-processor Gmsh (Geuzaine & Remacle, 2009). These are then connected to a number of parent structures, such that each does not exceed the number of DOFs of the child partitions. Eventually, the parent structures can become child partitions for a subsequent level of partitioning. The process goes on until the Level-0 parent structure has a number of DOFs comparable with that of any subdomains. The partitioning strategy is illustrated in Figure 3.

2.3 Mesh tying method

The mesh tying method allows for the connection of two structural components modelled independently with non-conforming meshes. Whereas this is a problem of large practical interest in mesoscale modelling of masonry structures (for instance when modelling the interface between backfill and masonry elements in bridges (Tubaldi, et al., 2018)), in this work it was deemed necessary for the connection of orthogonal walls and walls to floor, where an actual discontinuity was present for construction reasons (Figure 4).

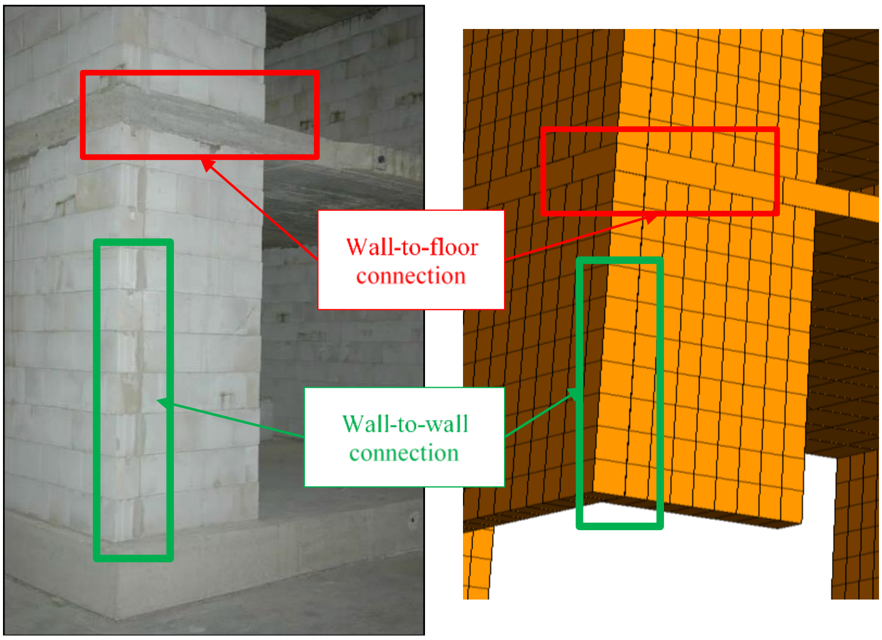

Figure 4. Non-conforming mesh connection.

The mesh-tying implemented in the nonlinear finite element analysis program ADAPTIC (Izzuddin, 1991) is based on a two-field formulation and the principle of mortar method constraint discretisation (Minga, et al., 2018). From a practical point of view, the two surfaces in contact are respectively defined as master and slave, where generally the master surface is characterised by larger size mesh and can be externally constrained, for instance by means of kinematic restraints or partition boundary enforcement. Given the master-slave surface definition, in a pre-processing phase a set of master elements is associated to each slave element, where such association is made if their areas overlap. To avoid over-constraining, only nodes belonging to the master surface can be externally constrained.

In order to consider possible failure for the connected surface, nonlinear interfaces, referred later to as wall-wall and wall-floor interfaces, were introduced in series with mesh tying.

2.4 Mesh creation

Considering all the features of the approach described above, the developed procedure for mesh creation aimed at the analysis of a realistic URM structure (i) enables the definition of the masonry bond and creation of the corresponding model in a semi-automatic way; (ii) includes the possibility of defining partitions, possibly hierarchically; and (iii) allows the connection of substructures with non-conforming meshes by means of mesh-tying.

Gmsh (Geuzaine & Remacle, 2009) was used as pre-processor for the creation of the basic mesh, thanks to its scripting capabilities and partitioning features. The process to create a masonry wall is illustrated in Figure 5 with reference to a typical English bond. Every planar masonry element is generated by means of triple extrusion (in x- y- and z direction), according to the patterns defined by the unit and joint dimensions. The elements generated in this way can be grouped according to their occurrence in the extrusion: odd/even in x direction, odd/even in y direction, odd/even in z direction, with a total eight groups. Some of the groups are to be discarded because, as intersection of extrusion directions, they must not be represented in the mesoscale approach (Figure 5). The retained elements will represent either units, bed joints or vertical interfaces. The application of the relevant masonry bond will consist of further subdividing this latter group in head joints and brick-brick interfaces.

This concept allows for the easy creation of walls with arbitrary dimensions and any kind of masonry bond within Gmsh. By re-writing the routine related to the triple extrusion, curved shapes can also be built (arches, vaults).

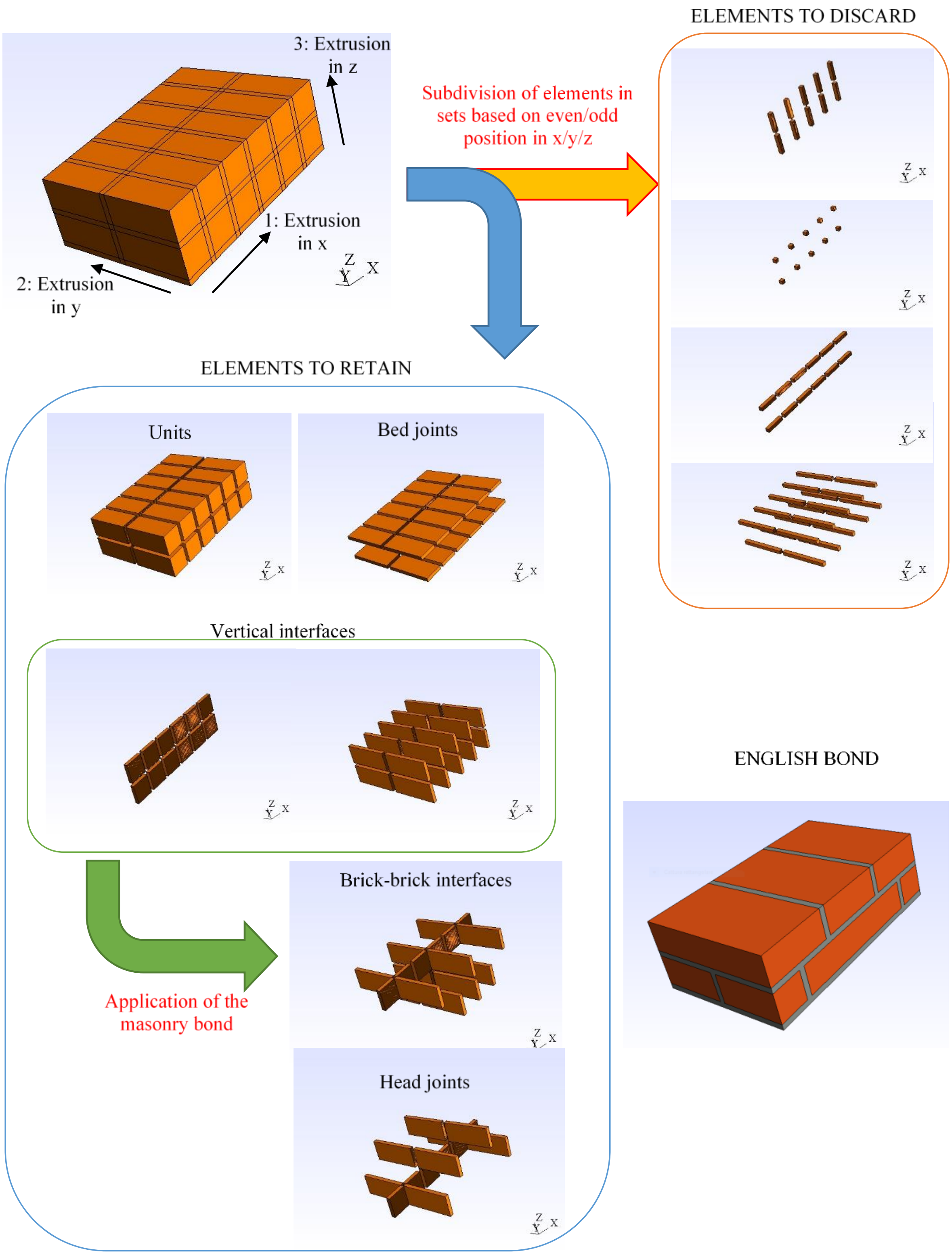

Figure 5. Automatic creation of mesoscale mesh for URM: application to an English bond.

Several partitioning algorithms, within Metis (Karypis & Kumar, 1998), or Chaco (Hendrickson & Leland, 1995) partitioners, are included in Gmsh, allowing for automatic subdivision of the domain in smaller partitions. An ad-hoc converter has been created to link the created mesh to ADAPTIC, performing the following operations:

- Including several mesh files (related for instance to different walls or floors) into a single model, by either detecting coincident nodes or applying correctly mesh-tying constraints as described in Section 2.3. The creation of independent walls or floors entails a simple and scalable generation of complex buildings;
- Collapsing the solid elements corresponding to bed joints and vertical interfaces (Figure 5) into zero-thickness interface elements, not present in Gmsh;
- Creating hierarchical partitioning graph from the basic partitions. This is shown in Figure 3;
- Writing the files in the correct format for ADAPTIC.

This process has been applied for the simulations described in the following sections.

3 Experimental tests

The experimental tests considered in this work were previously carried out within the FP6 European project "ESECMaSE - *Enhanced Safety and Efficient Construction of Masonry Structures in Europe*". The main aim of the ESECMaSE project was to develop a better understanding of the stress states in typical masonry structures by means of extensive testing activities. This has allowed the creation of a remarkable database of consistent results that has been considered in the present work to evaluate the ability of mesoscale modelling approach to accurately predict structural response at different scales. Herein, only masonry made of calcium silicate units is considered. The tests performed on this type of masonry were:

- Material tests on single constituents;
- Static shear tests on walls with different size ratios, boundary conditions and compression levels;

- Hammer tests on a building prototype for the estimation of the fundamental frequencies;
- Pseudo-dynamic tests on the building prototype.

The key results are briefly reported in the following subsections.

3.1 Materials

All walls were made of 250mm×175mm×250mm calcium silicate units of type 6DF optimised for the project. The units were assembled with thin mortar bed joints, while the head joints remained unfilled, with the out-of-plane connection being ensured by the matching vertical grooves. Compression and tensile tests on units and small assemblage were performed, providing the mechanical properties listed in Table 1.

Table 1. Mechanical properties of units and joints.

Material	Property	Value
Unit	Young's modulus	13620 MPa
	Poisson's ratio	0.253
	Compressive strength	23.6 MPa
	Tensile strength	1.49 MPa
Joint	Young's modulus	2849 MPa
	Poisson's ratio	0.028
	Tangent of friction angle	0.55
	Cohesion	0.28 MPa

3.1.1 Static tests on walls

In-plane cyclic testing on masonry piers was performed at the University of Pavia (Magenes, et al., 2008). An appropriate experimental setup was designed to simulate double fixed or cantilever boundary conditions while applying constant vertical loads and displacement-controlled horizontal cyclic loads with increasing displacement amplitude at the top of the walls. Four representative tests have been considered for the numerical simulations and their characteristics are reported in Table 2.

Table 2. Cyclic shear tests on specimens

Label	Dimensions [mm^3]	Vertical load [MPa]	Boundary conditions	Maximum horizontal load [kN]
CS02	1250×175×2500	1.0	Double fixed	87.56
CS03	1250×175×2500	0.5	Double fixed	49.25
CS06	1250×175×2500	1.0	Cantilever	43.57
CS07	2500×175×2500	1.0	Double fixed	226.08

3.2 Tests on the building prototype

With the aim of verifying the earthquake performance of a 2-storey terraced house with a rigid base and two RC floor slabs, seismic testing of a full-scale prototype was performed at the ELSA Reaction-wall Laboratory of the JRC, using pseudo-dynamic testing techniques (Anthoine & Capéran, 2008). The specimen, with global dimensions of 5.30m×4.75m and a height of 5.40m, represented one symmetric half of a house with a width of 5.30 m (Figure 6). The concrete slabs were poured directly on the units at the levels of the two floors without any mortar joint. Each shear wall was connected to the perpendicular long walls through a continuous vertical mortar joint with masonry connectors (i.e. metal strips) inserted in the mortar bed joints.

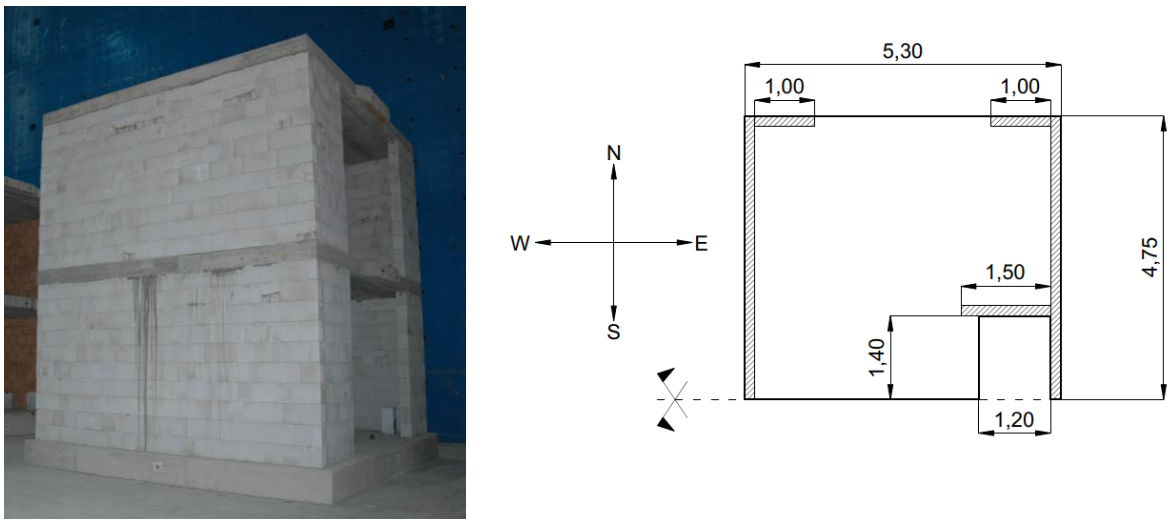

(a) (b)

Figure 6. Pseudo-dynamic test: (a) view of the structure (courtesy of Dr Armelle Anthoine), and (b) plan view.

The pseudo-dynamic tests were carried out under the vertical loading conditions used in the seismic design, that is, according to Eurocode 8, under the dead loads and 30% of the live loads. A distribution of water tanks on each floor was designed to account for the required dead and live loads and the specific testing set-up. The tanks were distributed so that the gravity loads on the masonry walls were the closest to the values expected in the original terraced house. Globally, the added masses summed up to 4521kg at the first floor and 7391kg at the second floor.

Before performing the pseudo-dynamic tests, a preliminary hammer test was carried out to identify modes, frequencies and damping. In this case, not all the masses used later for the pseudo-dynamic tests were in place, but only the additional masses inherent to the testing set-up, which consisted of 1603kg at the first floor and 1303kg at the second floor. The modal characteristics determined in the test are reported in Table 3. Later, the fundamental frequency in the E-W direction was further estimated as 6.3Hz by using measurements obtained during the first pseudo-dynamic test, thus still in undamaged conditions (Michel, et al., 2011).

Table 3. Modal characteristics of the structure.

Vibration mode	**Frequency [Hz]**	**Damping [%]**
E-W translation	8.03	0.85
N-S translation	16.63	1.35
Bending of the 2nd floor	19.02	1.00
Bending of the 1st floor	21.33	1.32
Torsion	21.46	1.36
Bending of the free wall	24.11	0.96

The pseudo-dynamic tests were unidirectional in the E-W direction (Figure 6b, in the following also referred to as longitudinal direction) and thus, in the pseudo-dynamic algorithm, the tested structure had two degrees of freedom only, one translation at each floor level. The movement of each floor slab was controlled by a pair of hydraulic actuators fixed on both sides and imposing the same horizontal displacement to prevent any rotation around a vertical axis. The test specimen being not symmetric, the forces required to reach a given displacement at a floor level differed in the two actuators but only their sum was necessary for the pseudo-dynamic algorithm. The mass matrix for the pseudo-dynamic test was selected as a 2×2 diagonal matrix with m_1=29t for the first floor and m_2=26.2t for the second floor. No viscous damping was introduced in the pseudo-dynamic algorithm.

The reference accelerogram was a 10.23s long artificial time history generated to match the EUROCODE 8 (EN 1998-1-1, 2005) design spectrum with elastic response spectrum type I, peak ground acceleration PGA=0.04g and soil type B. A series of scaled ground motions with increasing intensity (0.02g, 0.04g, 0.06g, etc. until 0.20g) was applied to the specimen. The first significant damages were reported to appear during the 0.12g test, and thus this has been used as reference for the simulations described in this work. The accelerogram of this test is shown in Figure 7.

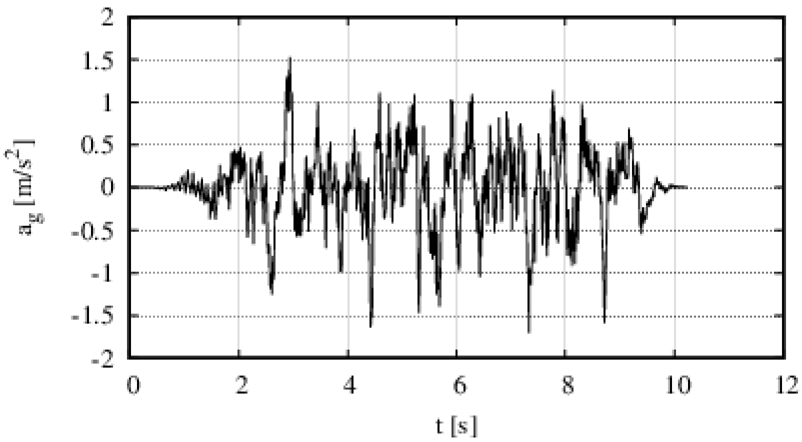

Figure 7. 0.12g scaled accelerogram for the pseudo-dynamic test.

Detailed description of the experimental setup and outcomes may be found in (Anthoine & Capéran, 2008). The main observations during the 0.12g test will be described in Section 4 along with the numerical results to enable a comparison between them.

4 Simulations and results

4.1 Material properties

The material properties for the simulations were defined based on the outcomes of ESECMaSE project and are listed in Table 4. Brick Young's modulus and Poisson's ratio were directly obtained by tests on single bricks. Normal elastic stiffness of bed joint interfaces was evaluated considering the deformability of masonry as provided by the ESECMaSE experimental reports and assuming that units and mortar worked as springs in series:

$$k_N = \left[h_b\left(\frac{1}{E_m} - \frac{1}{E_b}\right)\right]^{-1} \tag{3}$$

where h_b is the brick height, E_m and E_b the measured Young's moduli of masonry and bricks respectively. Shear stiffness was estimated based on approximate formula (rigorously only valid for Young's modulus of solids) $k_V = k_N/[2(1 + \nu_j)]$ with ν_j Poisson's ratio of joints. Bed joint tensile strength, cohesion, friction angle and brick tensile strength were determined by material tests performed during ESECMaSE project. The compressive strength of masonry, which is associated with a complex response characterised by triaxial stress states in masonry units and mortar joints, cannot be explicitly predicted by the proposed mesoscale representations using standard interface elements which do not allow for Poisson's effects. Thus it was considered here from a phenomenological point of view as compressive strength of all the interfaces (Macorini & Izzuddin, 2011). Lacking any experimental data, the damage parameter, brick-brick cohesion and friction angle, and all fracture energies were assigned values taken from the literature (Minga, et al., 2018; Chisari, et al., 2018). In particular, values for mortar joint fracture energy are consistent with experimental findings (CUR, 1994). It must be pointed out that fracture energy in shear is strongly dependent on the type of masonry and compression level (Chaimoon & Attard, 2005; Ravula & Subramaniam, 2019; Pluijm, et al., 2000). The value 0.2 N/mm adopted here is within the bounds highlighted by those authors.

Compressive fracture energy (for both brick and bed joint interfaces) was estimated as dependent from the compressive strength according to the relationship $G_{f,c} = 15 + 0.43f_c - 0.0036f_c^2$ as suggested in (Lourenço, 2009). In addition, unfilled head joints were considered having pure friction contact behaviour with same friction coefficient as bed joints, while the wall-wall and the wall-floor connections (for the tests on the building) had the same properties as brick-brick and bed joint interfaces, respectively. The compression strength of the brick-brick interface represents failure of units, while the compression strength of the bed joint interface represents failure of masonry for loading in the vertical direction.

Table 4. Material properties used in the simulations. Source label is: E=experimental, L=literature.

Parameter	Value	Source	Parameter	Value	Source
Brick Young’s modulus	13620 MPa	E			
Brick Poisson’s ratio	0.253	E			
Concrete Young modulus	30000 MPa	L			
Concrete Poisson’s ratio	0.15	L			
Bed joint axial stiffness	68.0 N/mm^3	E	Brick-brick axial stiffness	10^4 N/mm^3	L
Bed joint shear stiffness	33.1 N/mm^3	E	Brick-brick shear stiffness	10^4 N/mm^3	L
Bed joint tensile strength	0.35 MPa	E	Brick-brick tensile strength	1.49 MPa	E
Bed joint cohesion	0.28 MPa	E	Brick-brick cohesion	2.235 MPa	E
Bed joint friction angle	atan(0.55)	E	Brick-brick friction angle	atan(1.0)	L
Bed joint fracture energy (mode I)	0.01 N/mm	L	Brick-brick fracture energy (mode I)	0.1 N/mm	L
Bed joint fracture energy (mode II)	0.2 N/mm	L	Brick-brick fracture energy (mode II)	0.5 N/mm	L
Bed joint fracture energy (compression)	23.1 N/mm	L	Brick-brick fracture energy (compression)	23.9 N/mm	L
Bed joint damage parameter	0.1	L	Brick-brick damage parameter	0.1	L
Bed joint compressive strength	23.6 MPa	E	Brick-brick compressive strength	26.5 MPa	E

4.2 Tests on walls

The four specimens described in Table 2 were modelled according to the mesoscale strategy described above. A stiff element was also applied on the top of the walls to transfer the vertical load. The element was constrained to remain horizontal for specimens CS02, CS03, CS07 in order to simulate the double-fixed experimental setup. Dynamic analyses were performed to simulate the quasi-static cyclic tests because the addition of inertia forces (corresponding to the actual masses of the walls) in the simulation facilitates the attainment of convergence. A comparison between experimental and computed force-displacement plots at the top of the walls is shown in Figure 8.

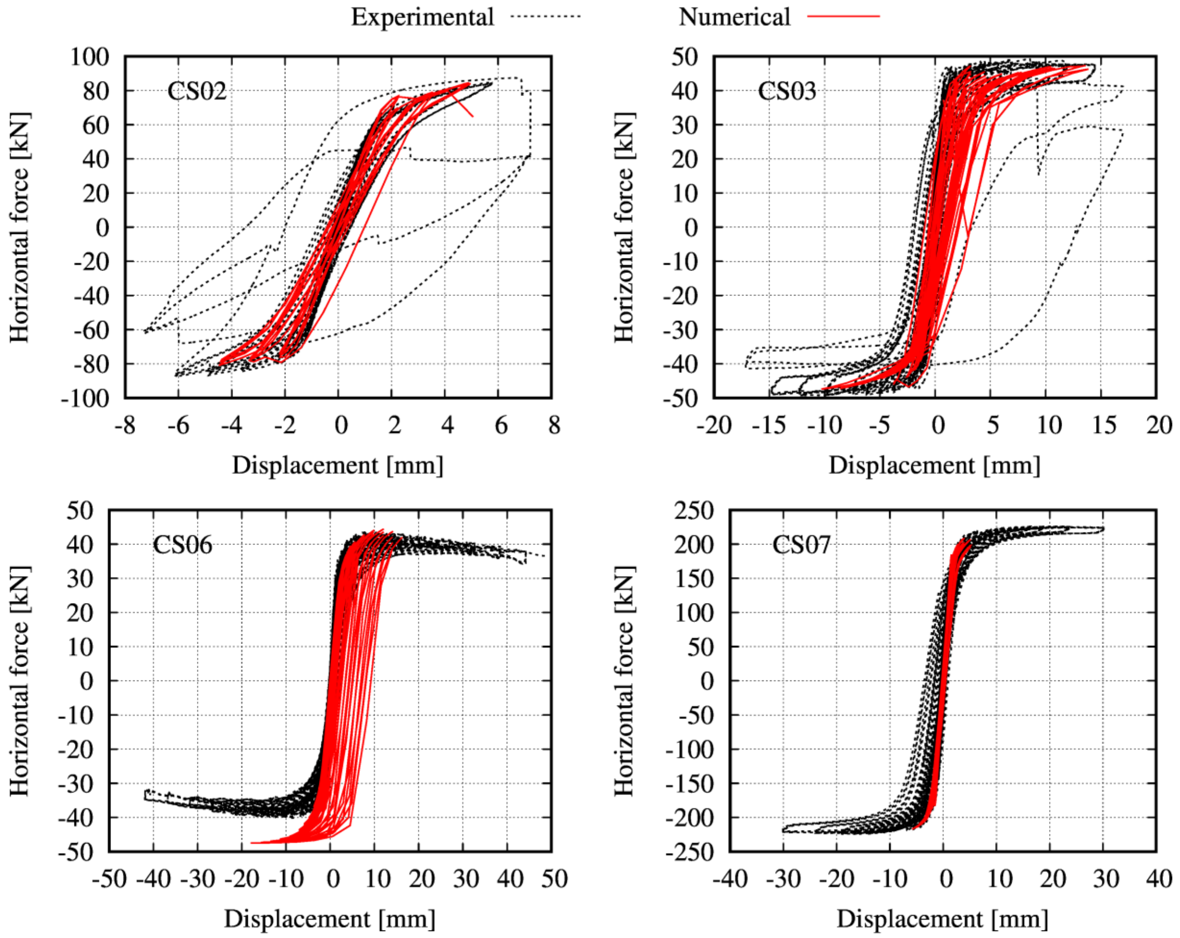

Figure 8. Experimental-computed force-displacement plots for the shear tests on walls.

Taking CS02 as reference, it is possible to see that halving the vertical load (CS03) or removing the constraint on the top (CS06) have similar effect of halving the maximum horizontal strength of the specimen. Doubling the width of the panel (CS07) entails a 158% increase in strength.

Concerning the hysteretic energy dissipation capacity, all specimens were characterised by symmetric S shape of the plot, no strength degradation and low levels of dissipation. These are indications of rocking behaviour of the specimens. Generally, the computed response is close to the experimental tests, in terms of stiffness, strength and hysteretic behaviour. In the case of specimen CS06, the numerical model suffered from a loss of symmetry and started moving towards one side as an effect of cumulated shear plastic strain. This affected the symmetry of the envelope shown in Figure 8. The simulation of tests CS06 and CS07 could not reach the maximum displacements due to convergence problems. The final crack patterns for experimental and numerical tests are shown in Figure 9 and Figure 10 respectively.

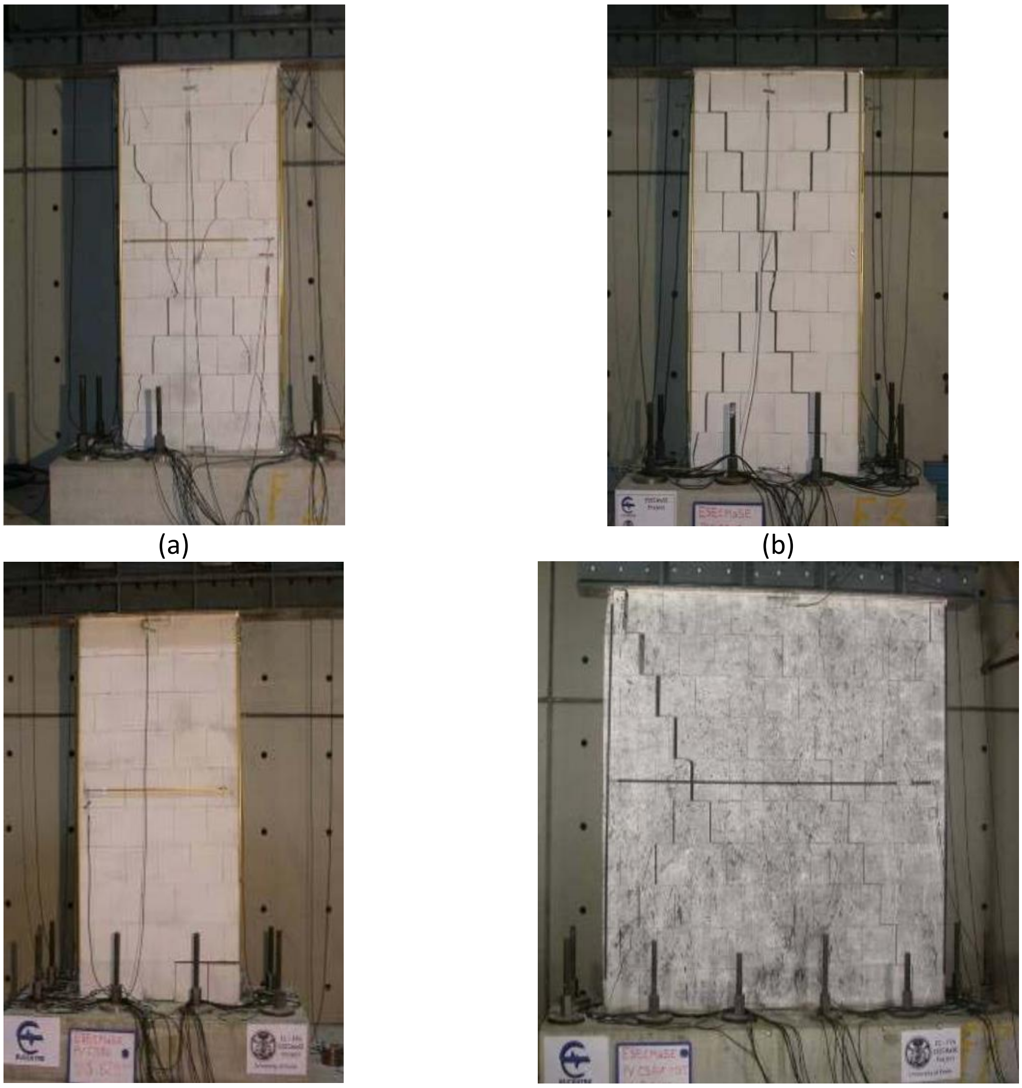

(a) (b) (c) (d)

Figure 9. Experimental crack patterns for the walls subjected to shear test: (a) CS02, (b) CS03, (c) CS06, (d) CS07 (from (Magenes, et al., 2008)).

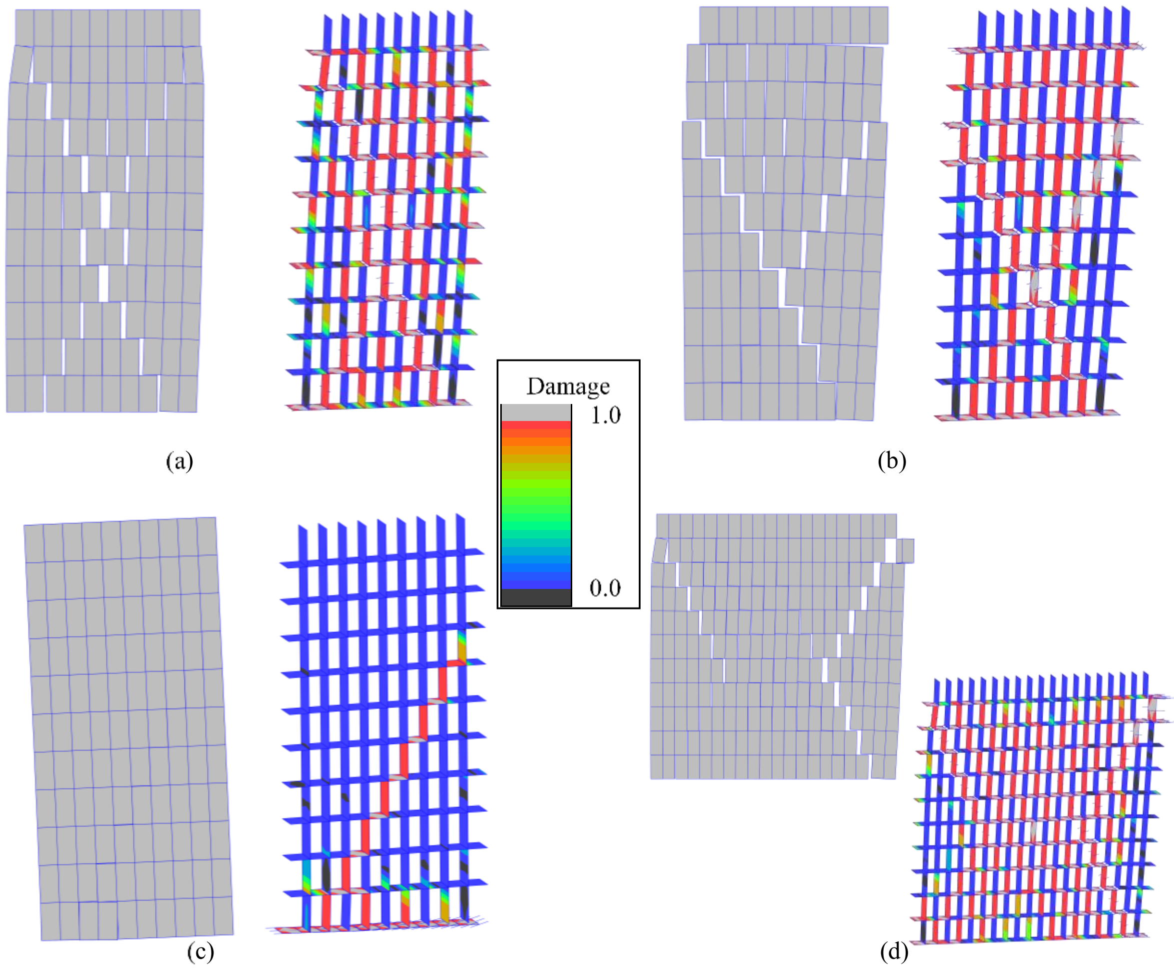

Figure 10. Numerical crack patterns and damage contours in the interfaces for the walls subjected to shear test: (a) CS02, (b) CS03, (c) CS06, (d) CS07.

The results show generally good agreement in terms of cracking pattern for all the specimens. In the case of the CS03 wall, the diagonal crack starts from below the second brick row from top, while experimentally the major crack was observed starting from the top. Clearly, there the response can be strongly influenced by the local conditions of the interface between loading beam and the wall, which in the simulation has been modelled with the same interface type as the ordinary bed joints. In the numerical simulation, specimen CS06, whose boundary conditions were those of cantilever beam, experienced complete loss of bond at the bottom interface due to tensile failure. This led to accumulation of shear plastic strain at the bottom which forced the specimen to move spuriously on one side. This spurious asymmetry reflected to the final damage pattern in the interfaces (Figure 10c) where an asymmetrical diagonal crack developed. Given that this behaviour occurred when the cantilever panel had completely lost strength to horizontal actions, this should not be a concern in general cases where such state is unlikely to emerge.

4.3 Parametric analysis

With the aim of exploring the effects of the most relevant material parameters, a parametric analysis was performed on specimen CS02. A simplified loading history characterised by a single half-cycle loading with maximum displacement equal to 6mm was applied to the specimen. Keeping the model used for the simulation of the experimental tests as reference, the most relevant nonlinear material parameters were varied within a realistic range (Table 5).

Table 5. Variation ranges used for the parametric analysis.

Parameter	**Symbol**	**Range**
Bed joint cohesion	c	0.2-0.5 MPa
Bed joint friction coefficient	$\tan\phi$	0.55-0.9
Bed joint tensile strength	f_t	0.2-0.4 MPa
Bed joint fracture energy (mode I)	G_t	0.005-0.02 N/mm
Bed joint damage parameter	μ	0.1-1.0

The results in terms of force-displacement curves are displayed in Figure 11a-e. From the plots, it is clear that the variation of the parameters only slightly affects the monotonic behaviour; conversely the unloading path, and thus energy dissipation, unloading stiffness and residual displacement at unloading, are strongly dependent upon them. Three main failure modes were observed for the structure: flexural (F), with opening of horizontal cracks at the top and bottom interfaces; shear (S), with opening of diagonal cracks following the mortar joints; and a mixed mode (SF). The actual failure mode is indicated in the plots with the corresponding label. Shear failure modes are generally characterised by higher energy dissipation, while flexural modes show a reduced dissipative behaviour which is characteristic of rocking motions. The only notable exception is the variation of μ (plot e), governing the amount of residual plastic strain in the material model, which allows for increased energy dissipation by maintaining a flexural failure mode. It is possible to appreciate that, except for the variation due to c (plot a) and to μ (plot e), there is no monotonic trend in the dissipation characteristics (energy and residual displacement). This can be explained by the observation that in all cases, except for plot (e), a variation in the parameter value also leads to a variation in failure mode, losing monotonicity in the response.

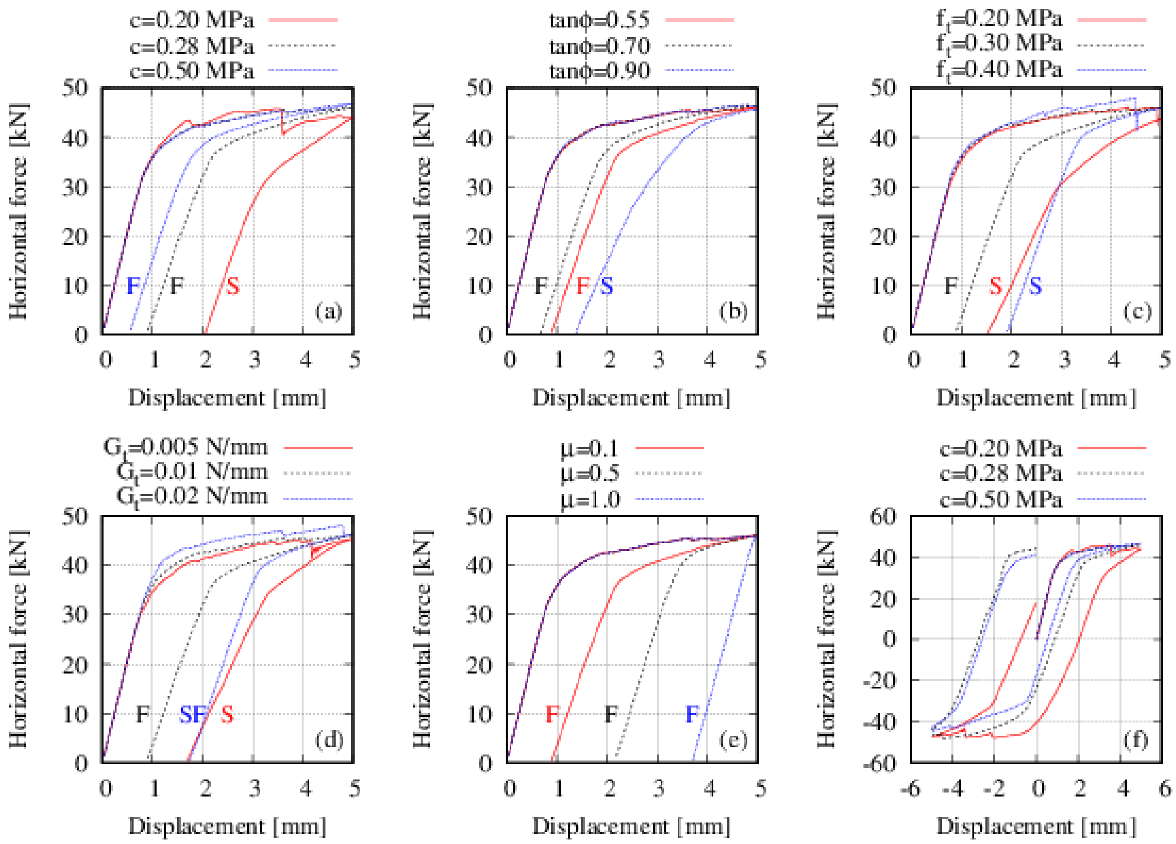

Figure 11. Force-displacement plots of the parametric analysis: (a) variation with c, (b) variation with tanϕ, (c) variation with f_t, (d) variation with G_t, (e) variation with μ, (f) full cycle for models in (a). The labels indicate the failure mode: F (flexural), S (shear), SF (mixed).

Furthermore, it must be pointed out that what is observed in a half-cycle may not be representative of the overall behaviour of the structure under full cycling loading. As an example, the larger dissipation observed in Figure 11a for low values of cohesion is not evident anymore if we consider a full cycle (Figure 11e). This is explained by a switch in failure mode (from flexural to shear) due to coupling between tensile and shear damage in the material model for the interface: in other words, after being damaged in tension due to the opening of the flexural crack, the top interface loses cohesion upon loading reversal and the failure mode is turned into sliding between the loading application beam and the wall. This is a further demonstration of the complexity of the mechanical behaviour of masonry and the possibility offered by the adopted mesoscale model in terms of its representation.

4.4 Seismic analysis of the building

The finite element model of the building, developed as described in Section 2, consists of 73 basic partitions, each with ~2200 DOFs on average. The overall model consisted thus of 161,748 DOFs. Higher rank partitions were created up to three levels (see Figure 3) broadly keeping the same number of DOFs per partition, creating an overall model made of 87 partitions including the parent structure. The calculations were then parallelised on 4 nodes of the High-Performance Computing facilities at Imperial College London, made of 24 processors each.

A preliminary modal analysis was performed to compare the dynamic characteristics of the model with those estimated in the laboratory by means of the hammer test. Lanczos algorithm was utilised for the solution of the eigenvalue problem. The mass setup described in Section 3.2 was represented in the model as density distribution within the solid elements of each floor, while the wall units were assigned their density equal to $2 \cdot 10^{-6}$ kg/mm^3.

Globally, the modal shapes obtained by the eigenvalue analysis correspond to those estimated by means of the hammer test (Figure 12), even though some mode switch occurred (the global torsional mode had the fifth smallest frequency in the test, against the third in the numerical simulations). The numerical frequencies are slightly smaller than the experimental counterparts, but this is acceptable as, given the low amplitude of the induced vibrations, the hammer tests are expected to give frequency upper bounds (Anthoine & Tirelli, 2008).

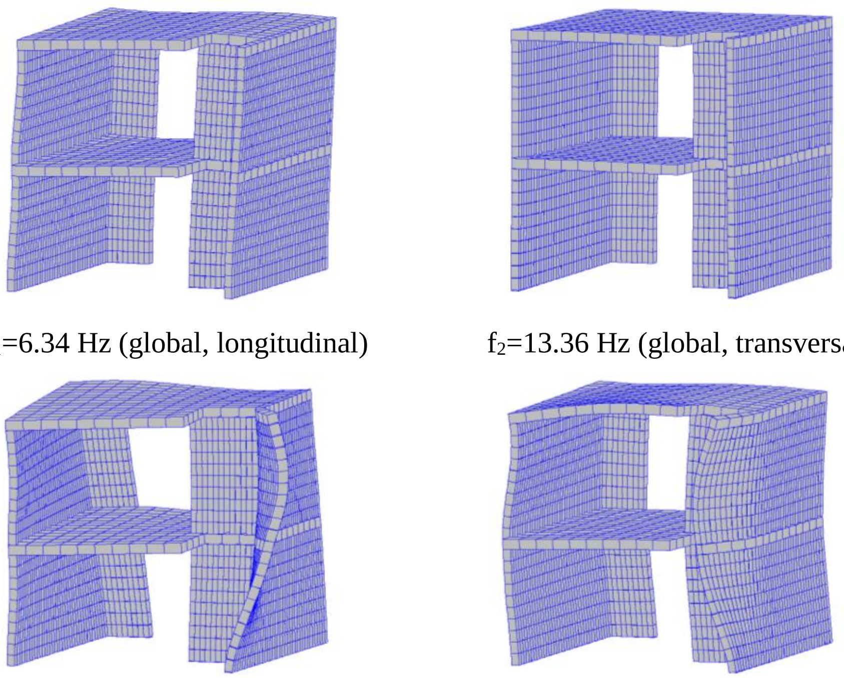

f_1=6.34 Hz (global, longitudinal) f_2=13.36 Hz (global, transversal)

f_3=16.81 Hz (global, torsional) f_4=19.04 Hz (local, bending of the second floor)

Figure 12. Numerical modes of vibration of the structure.

The pseudo-dynamic experimental test was simulated by means of a dynamic analysis in which the acceleration history displayed in Figure 7 (and thus scaled to PGA=0.12g) was applied to the ground nodes in the E-W direction. This level of ground motion acceleration was selected as it was experimentally observed that for this analysis the first significant damage appeared on the structure. Self-weight and additional weight were implemented as initial loads to the structure, and the corresponding masses present on the real specimen were simulated by either density of solid elements or lumped mass elements. No damping was considered, in line with the pseudo-dynamic test assumptions (Anthoine & Capéran, 2008). The Hilber-Hughes-Taylor integration scheme with α=-0.33, β= 0.25(1-α)^2, γ=0.5-α was employed for the solution of the dynamic problem. The initial time increment was 0.005s, i.e. half the accelerogram time step, but up to 3 levels of sub stepping with factor 0.1 when convergence is not attained are allowed by ADAPTIC.

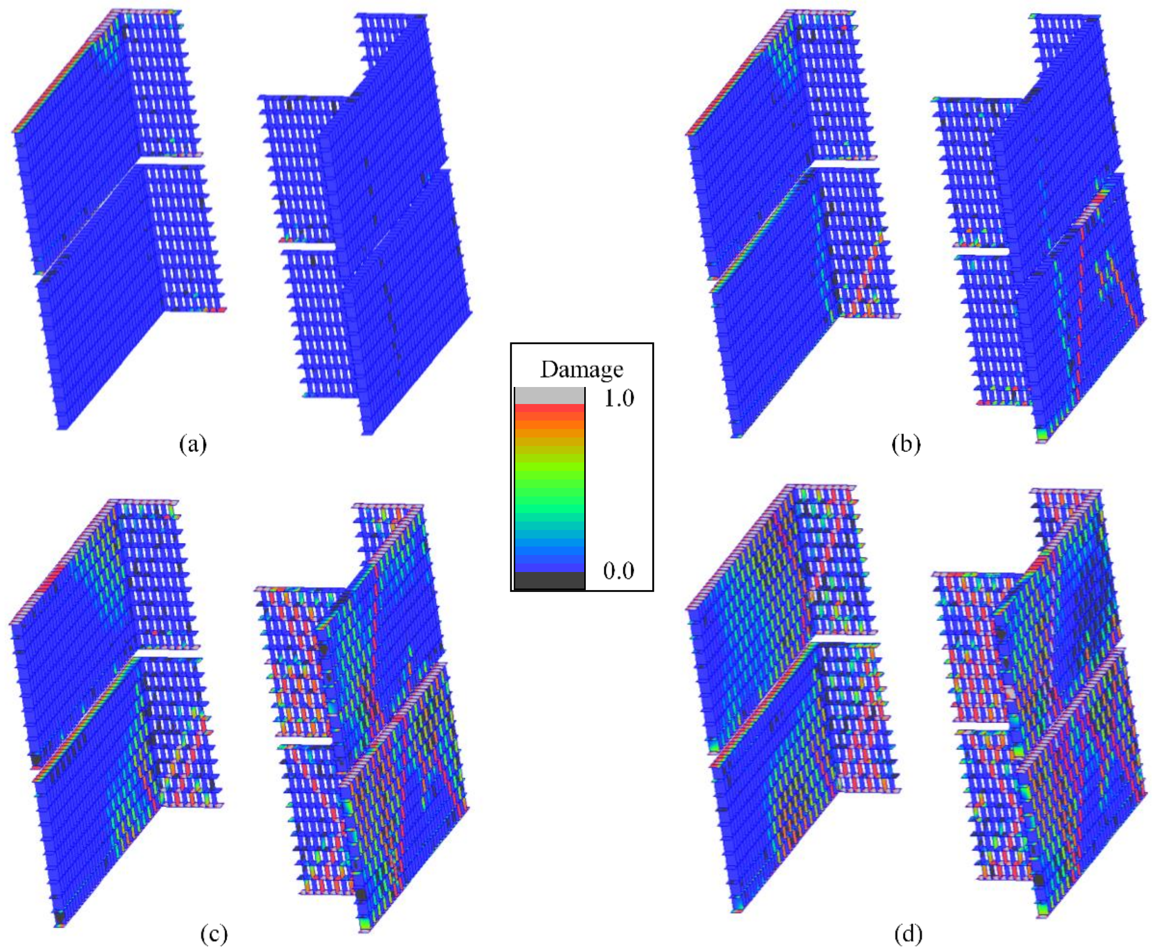

Figure 13. Evolution of damage in tension in the interfaces: (a) after 2.0s, (b) after 3.0s, (c) after 5.0s, and (d) at the end of the analysis.

Figure 13 shows the evolution of the damage in the structure with time. Damage variables are a measure of the ratio of the plastic work performed at the integration point by internal stresses and the relevant fracture energy. Already in the first phases of the analysis, some damage due to flexural cracks appears at the interface between floors and walls in the transversal west long wall, eventually propagating to the upper corner part of the wall. At 3.0s, after the first acceleration peak, diagonal damage appears in the longitudinal short walls and in the east long wall. Detachment between floor and wall is also observed there. At 5.0s, after the second acceleration peak, the building results extensively damaged in all its parts: shear resisting mechanisms are induced in the short walls, while these interact with the long walls provoking large damage near the connections. This typology of damage remains until the end of the analysis, eventually spreading into the walls (Figure 13d).

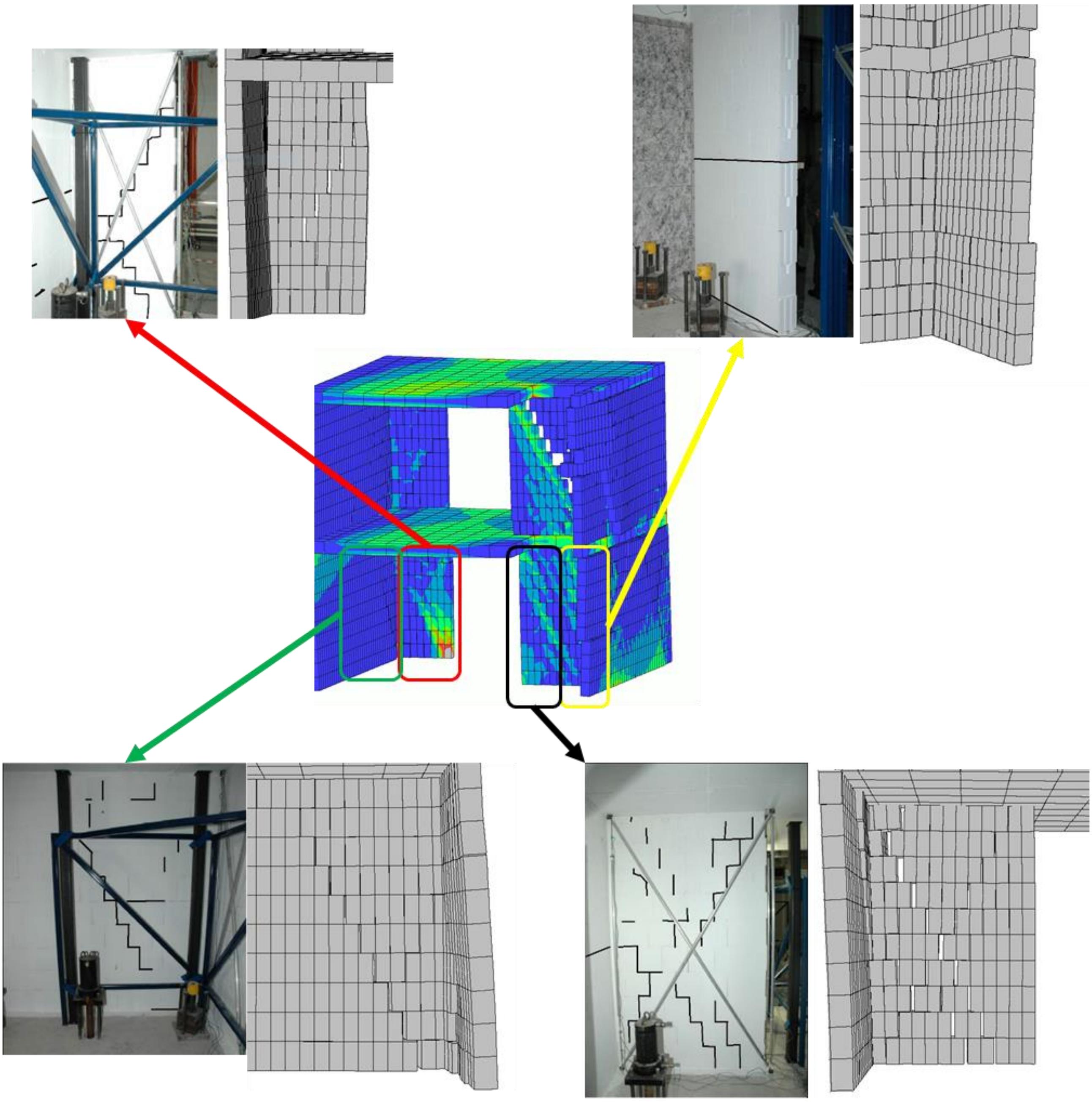

Figure 14. Comparison between experimental observations and numerical simulation of cracks at the end of the test. Displacements are magnified 20 times.

In Figure 14, a visual comparison between cracks observed experimentally and the numerical simulation is shown. In the experimental tests, it is reported that in both long transversal walls, a horizontal crack opened at the mid-height of the first level (Anthoine & Capéran, 2008). This is also observed in the numerical model at the end of the analysis (Figure 14 top-right). Large stepwise diagonal cracks were observed in the shear walls at the ground floor, and generally well reproduced by the numerical model.

Finally, a comparison between experimental and numerical base shear-floor displacement plots is shown in Figure 15.

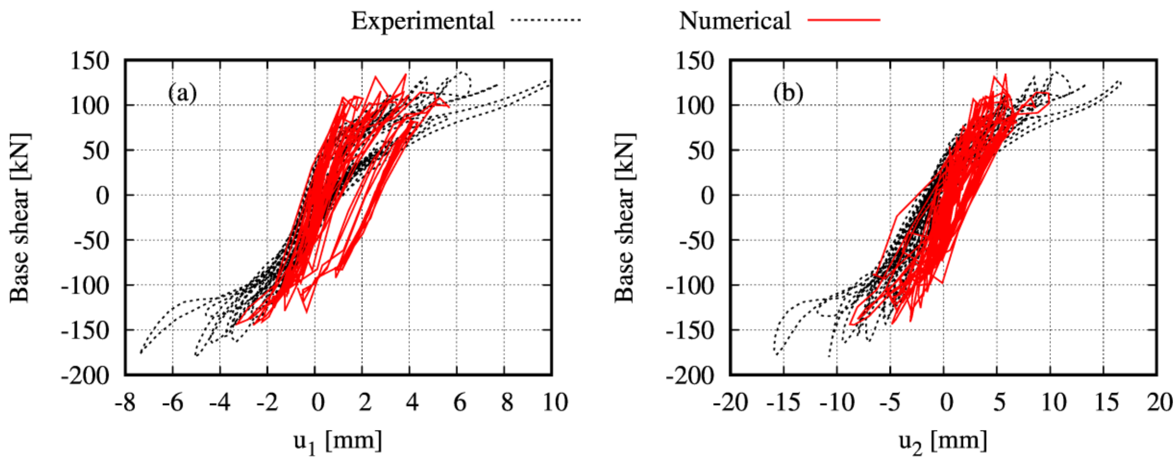

Figure 15. Experimental-numerical base shear-floor displacements: (a) first floor displacement, and (b) second floor displacement.

The results show that remarkable agreement with the experimental results is obtained in the simulation as far as the maximum base shear and overall stiffness is concerned. The top displacement reached 10mm, which is slightly less than the experimental 16.6mm. This is believed to be due to three main causes. The first one is that the actual test was a pseudo-dynamic test, while the simulation applied the ground motion at the base of the structure. This implies that some approximations are present, e.g. in masonry structures wall mass is significant, but in the pseudo-dynamic algorithm the mass was assumed concentrated at the floors. Secondly, an increasing level of damage was experimentally observed in the tests preceding the 0.12g test, as the initial frequency value estimated from the identification results dropped from 6.3Hz of the first test at 0.02g to 5.6Hz for the test at 0.12g (Michel, et al., 2011). This 11% frequency reduction is due to some accumulated damage that the structure underwent during the previous tests but which was not simulated, as in the analysis the building was subjected to the 0.12g ground motion in undamaged conditions, due to lack of detailed information on initial damage. Finally, it is noted that some experimental values for the material properties were not available and are based on literature assumptions. In particular, fracture energy properties may significantly affect the local post peak behaviour of interfaces and thus can have a role in the stress redistribution following the elastic branch, and ultimately on the response of the structure in terms of ductility.

5 Conclusions

In this paper, some tests performed within a previous European project have been simulated by means of an advanced mesoscale strategy entailing a damage-plastic material model for interfaces representing possible cracks, hierarchic partitioning of the FE model and tying of non-conforming meshes. The strategy includes a methodology aimed at accurate analysis of the seismic behaviour of masonry buildings which has been developed to easily create the finite element building model considering any masonry bond and connection between walls.

Calibration of material properties has been carried out considering the material tests available and some literature assumptions. No further adjustments to fit the experimental response was then performed, with the aim of assessing the strategy including the difficulties of calibrating the large number of material parameters involved.

The application of cyclic tests on single walls subjected to different loading and constraint conditions shows a remarkable agreement between experimental and numerical results, either in terms of crack pattern, stiffness, maximum strength and hysteretic behaviour. In particular, the typical rocking behaviour of the specimens under damaged conditions, highlighted by the

S-shaped force-displacement plot and absence of strength degradation is well represented by the model. It is underlined here that such rocking behaviour appears in case of either flexural or shear cracking patterns.

A parametric analysis on the influence of the main material parameters has been performed considering one of the wall previously simulated. The results show the complexity of the response of masonry under cyclic loading, where failure mode switch can occur due to coupling between different types of damage.

The strategy is then applied for reproducing the seismic behaviour of a full-scale building subjected to ground motion acceleration. Modal properties are generally shown to comply with the experimental estimations obtained in hammer tests, even though some mode switching occurred, and the frequencies were found slightly smaller than the experimental counterparts. However, this was expected based on recommendations from other authors, given the low level of energy induced to the structure by the hammer test.

The dynamic analysis simulating the pseudo-dynamic test allows for a study of the damage evolution in the structure. Different damage mechanisms at macro-scale level can be recognised and simulated during the earthquake time history, from tensile failure at the wall-floor connection to the diagonal shear mechanisms of the walls resisting to the inertia forces. The experimental cracking pattern and the deformed shape of the numerical model show remarkable agreement, while it is suggested that more accurate calibration of the material model parameters and careful consideration of previous loading histories could lead to better predictions regarding the displacement history at the two storeys.

The results reported in this paper show that mesoscale strategy can be very effective in reproducing the seismic behaviour of masonry at wall and building scale. The drawback is represented by the computing demand, which has been mitigated in the present work through the use of High Performance Computing resources at Imperial College London, which are usually not available in the professional practice. To solve this issue, the results of this work are being further exploited in ongoing research in which less expensive macroscale modelling approaches will be connected to the described mesoscale methodology to create a multi-level procedure.

6 Data Availability Statement

Some or all data, models, or code used during the study were provided by a third party:

- Experimental data

Direct requests for these materials may be made to the provider as indicated in the Acknowledgements.

Some or all data, models, or code generated or used during the study are proprietary or confidential in nature and may only be provided with restrictions:

- ADAPTIC code (limited access may be provided upon request to the last author);
- Numerical models (they can be provided by contacting the first author).

7 Acknowledgements

The first author has been supported by the European Commission through the Marie Skłodowska-Curie Individual Fellowship “MultiCAMS – *Multi-level Model Calibration for the Assessment of Historical Masonry Structures*”, Project no. 744400. Dr Armelle Anthoine at the European Laboratory for Structural Assessment, Prof. Andrea Penna at the University of Pavia and the consortium of ESECMaSE project are gratefully acknowledged for providing the experimental data used in this research. Finally, the authors acknowledge the Research Computing Service at Imperial College for providing and supporting the required High-Performance Computing facilities.

8 References

Addessi, D. & Sacco, E., 2016. Enriched plane state formulation for nonlinear homogenization of in-plane masonry wall. *Meccanica,* 51(11), pp. 2891-2907.

Anthoine, A., 1995. Derivation of the in-plane elastic characteristics of masonry through homogenization theory. *International Journal of Solids and Structures,* 32(2), pp. 137-163.

Anthoine, A. & Capéran, P., 2008. *Earthquake tests and analysis of the experimental results,* European Laboratory for Structural Assessment (ELSA), Ispra (Italy): Deliverable 8.3 ESECMaSE project.

Anthoine, A. & Tirelli, D., 2008. *Preliminary tests and dynamic identification of the specimens,* European Laboratory for Structural Assessment (ELSA), Ispra (Italy): Deliverable 8.2 ESECMaSE project.

Berto, L., Saetta, A., Scotta, R. & Vitaliani, R., 2002. An orthotropic damage model for masonry structures. *Int J Numer Methods Eng,* Volume 55, pp. 127-157.

Betti, M., Galano, L. & Vignoli, A., 2014. Comparative analysis on the seismic behaviour of unreinforced masonry buildings with flexible diaphragms. *Engineering Structures,* 61(1), pp. 195-208.

Betti, M., Galano, L. & Vignoli, A., 2015. Time-History Seismic Analysis of Masonry Buildings: A Comparison between Two Non-Linear Modelling Approaches. *Buildings,* 5(2), pp. 597-621.

Chaimoon, K. & Attard, M. M., 2005. *Shear fracture in masonry joints.* Malta, WIT Press.

Chisari, C., Macorini, L., Amadio, C. & Izzuddin, B., 2018. Identification of mesoscale model parameters for brick-masonry. *International Journal of Solids and Structures,* Volume 146, pp. 224-240.

Chisari, C., Macorini, L., Amadio, C. & Izzuddin, B. A., 2015. An Inverse Analysis Procedure for Material Parameter Identification of Mortar Joints in Unreinforced Masonry. *Computers and Structures,* Volume 155, pp. 97-105.

CUR, 1994. *Structural masonry: a experimental/numerical basis for practical design rules,* Gouda, The Netherlands: CUR.

D’Ayala, D. & Ansal, A., 2012. Non linear push over assessment of heritage buildings in Istanbul to define seismic risk. *Bulletin of Earthquake Engineering,* 10(1), p. 285–306.

D'Altri, A. M. et al., 2019. A damaging block-based model for the analysis of the cyclic behaviour of full-scale masonry structures. *Engineering Fracture Mechanics,* Volume 209, pp. 423-448.

EN 1998-1-1, 2005. *Eurocode 8: Design of structures for earthquake resistance-Part 1: General rules, seismic actions and rules for buildings.*. s.l.:European Standard.

Endo, Y., Pelà, L. & Roca, P., 2017. Review of Different Pushover Analysis Methods Applied to Masonry Buildings and Comparison with Nonlinear Dynamic Analysis. *Journal of Earthquake Engineering,* 21(8), pp. 1234-1255.

Gambarotta, L. & Lagomarsino, S., 1997. Damage models for the seismic response of brick masonry shear walls. Part I: the mortar joint model and its applications. *Earthquake Engineering and Structural Dynamics,* 26(4), pp. 423-439.

Geuzaine, C. & Remacle, J.-F., 2009. Gmsh: a three-dimensional finite element mesh generator with built-in pre- and post-processing facilities. *International Journal of Numerical Methods in Engineering,* Volume 79, pp. 1309-1331.

Hendrickson, B. & Leland, R., 1995. *A multi-level algorithm for partitioning graphs.* San Diego CA (USA), Supercomputing - Proceedings of the IEEE/ACM SC95 Conference.

Izzuddin, B. A., 1991. *Nonlinear dynamic analysis of framed structures.* Imperial College London: PhD Thesis.

Jokhio, G., 2012. *Mixed dimensional hierarchic partitioned analysis of nonlinear structural systems.* Imperial College London: PhD Thesis.

Jokhio, G. A. & Izzuddin, B. A., 2013. Parallelisation of nonlinear structural analysis using dual partition super elements. *Advances in Engineering Software,* Volume 60, pp. 81-88.

Jokhio, G. A. & Izzuddin, B. A., 2015. A Dual Super-Element Domain Decomposition Approach for Parallel Nonlinear Finite Element Analysis. *International Journal for Computational Methods in Engineering Science and Mechanics,* 16(3), pp. 188-212.

Kallioras, S., Graziotti, F. & Penna, A., 2019. Numerical assessment of the dynamic response of a URM terraced house exposed to induced seismicity. *Bulletin of Earthquake Engineering,* 17(3), p. 1521–1552.

Karypis, G., 2015. *Family of Graph and Hypergraph Partitioning Software.* [Online] Available at: http://glaros.dtc.umn.edu/gkhome/views/metis [Accessed 21 01 2018].

Karypis, G. & Kumar, V., 1998. Multilevel k-way Partitioning Scheme for Irregular Graphs. *Journal of Parallel and Distributed Computing,* 48(1), pp. 96-129.

Kim, S.-C. & White, D. W., 2004. Nonlinear analysis of a one-story low-rise masonry building with a flexible diaphragm subjected to seismic excitation. *Engineering Structures,* 26(14), pp. 2053-2067.

Lagomarsino, S., Penna, A., Galasco, A. & Cattari, S., 2013. TREMURI program: An equivalent frame model for the nonlinear seismic analysis of masonry buildings. *Engineering Structures,* Volume 56, pp. 1787-1799.

Lourenço, P., 1996. *Computational strategies for masonry structures.* Technische Universiteit Delft: PhD Thesis.

Lourenço, P. B., 2009. Recent advances in masonry modelling: micromodelling and homogenisation. In: U. Galvanetto & M. H. F. Aliabadi, eds. *Multiscale Modeling in Solid Mechanics.* London: Imperial College Press, pp. 251-294.

Lourenço, P. B. & Rots, J. G., 1997. Multisurface Interface Model for Analysis of Masonry Structures. *Journal of Engineering Mechanics,* 123(7), pp. 660-668.

Luciano, R. & Sacco, E., 1997. Homogenization technique and damage model for old masonry material. *International Journal of Solids and Structures*, 34(24), pp. 3191-3208.

Macorini, L. & Izzuddin, B., 2011. A non-linear interface element for 3D mesoscale analysis of brick-masonry structures. *International Journal of Numerical Methods in Engineering,* Volume 85, pp. 1584-1608.

Macorini, L. & Izzuddin, B., 2013. Nonlinear analysis of masonry structures using mesoscale partitioned modelling. *Advances in Engineering Software,* Volume 60-61, pp. 58-69.

Macorini, L. & Izzuddin, B. A., 2013. *Enhanced mesoscale partitioned modelling for unreinforced masonry structures.* Cagliari (Italy), Civil-Comp Proceedings.

Macorini, L. & Izzuddin, B. A., 2014. Nonlinear Analysis of Unreinforced Masonry Walls under Blast Loading Using Mesoscale Partitioned Modeling. *Journal of Structural Engineering ASCE,* 140(8), p. A4014002.

Magenes, G., Morandi, P. & Penna, A., 2008. *Test results on the behaviour of masonry under static cyclic in plane lateral loads,* University of Pavia: Deliverable 7.1c ESECMaSE project.

Mandirola, M., Galasco, A., Penna, A. & Magenes, G., 2016. *Nonlinear macroelement modelling of experimental tests on masonry buildings with rigid diaphragms.* Padova (Italy), s.n.

Massart, T., Peerlings, R. & Geers, M., 2007. An enhanced multi-scale approach for masonry wall computations with localization of damage. *International Journal for Numerical Methods in Engineering*, 69(5), pp. 1022-1059.

Mendes, N. & Lourenço, P. B., 2014. Sensitivity analysis of the seismic performance of existing masonry buildings. *Engineering Structures,* Volume 80, pp. 137-146.

Michel, C. et al., 2011. Quantification of fundamental frequency drop for unreinforced masonry buildings from dynamic tests. *Earthquake engineering and structural dynamics,* Volume 40, pp. 1283-1296.

Milani, G. & Valente, M., 2015. Comparative pushover and limit analyses on seven masonry churches damaged by the 2012 Emilia-Romagna (Italy) seismic events: Possibilities of non-linear finite elements compared with pre-assigned failure mechanisms. *Engineering Failure Analysis,* 47(A), pp. 129-161.

Minga, E., Macorini, L. & Izzuddin, B., 2018. A 3D mesoscale damage-plasticity approach for masonry structures under cyclic loading. *Meccanica,* 53(7), pp. 1591-1611.

Minga, E., Macorini, L. & Izzuddin, B., 2018. Enhanced mesoscale partitioned modelling of heterogeneous masonry structures. *International Journal for Numerical Methods in Engineering*, 113(13), pp. 1950-1971.

Pantò, B., Cannizzaro, F., Caddemi, S. & Caliò, I., 2016. 3D macro-element modelling approach for seismic assessment of historical masonry churches. *Advances in Engineering Software,* Volume 97, pp. 40-59.

Pluijm, R. V. d., Rutten, H. & Ceelen, M., 2000. *Shear behaviour of bed joints.* Madrid, 12th International Brick and Block Masonry Conference (12th IBMAC).

Ravula, M. & Subramaniam, K. V. L., 2019. Experimental Investigation and Interface Material Model for the Cohesive–Frictional Shear Response of Soft-Brick Masonry under Applied Compression. *Journal of Materials in Civil Engineering*, 31(12), p. 04019311.

Sarhosis, V. & Sheng, Y., 2014. Identification of material parameters for low bond strength masonry. *Engineering Structures*, Volume 60, pp. 100-110.

Tubaldi, E., Macorini, L. & Izzuddin, B. A., 2018. Three-dimensional mesoscale modelling of multi-span masonry arch bridges subjected to scour. *Engineering Structures,* Volume 165, pp. 486-500.

Valente, M. & Milani, G., 2019. Damage assessment and collapse investigation of three historical masonry palaces under seismic actions. *Engineering Failure Analysis,* Volume 98, pp. 10-37.

Zhang, Y., Macorini, L. & Izzuddin, B. A., 2016. Mesoscale partitioned analysis of brick-masonry arches. *Engineering Structures,* Volume 124, pp. 142-166.